NANO LETTERS

pubs.acs.org/NanoLett Letter

# Dark-Exciton Driven Energy Funneling into Dielectric Inhomogeneities in Two-Dimensional Semiconductors

Haowen Su, Ding Xu, Shan-Wen Cheng, Baichang Li, Song Liu, Kenji Watanabe, Takashi Taniguchi, Timothy C. Berkelbach, James C. Hone, and Milan Delor*

Cite This: *Nano Lett.* 2022, 22, 2843−2850 Read Online

ACCESS | Metrics & More | Article Recommendations | Supporting Information

**ABSTRACT:** The optoelectronic and transport properties of two-dimensional transition metal dichalcogenide semiconductors (2D TMDs) are highly susceptible to external perturbation, enabling precise tailoring of material function through postsynthetic modifications. Here, we show that nanoscale inhomogeneities known as nanobubbles can be used for both strain and, less invasively, dielectric tuning of exciton transport in bilayer tungsten diselenide ($WSe_2$). We use ultrasensitive spatiotemporally resolved optical scattering microscopy to directly image exciton transport, revealing that dielectric nanobubbles are surprisingly efficient at funneling and trapping excitons at room temperature, even though the energies of the bright excitons are negligibly affected. Our observations suggest that exciton funneling in dielectric inhomogeneities is driven by momentum-indirect (dark) excitons whose energies are more sensitive to dielectric perturbations than bright excitons. These results reveal a new pathway to control exciton transport in 2D semiconductors with exceptional spatial and energetic precision using dielectric engineering of dark state energetic landscapes.

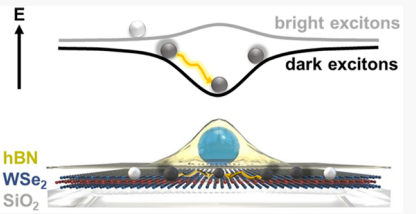


**KEYWORDS:** *exciton transport, 2D semiconductors, dark excitons, ultrafast microscopy, dielectric engineering, nanobubbles*



Two-dimensional transition metal dichalcogenide semiconductors (2D TMDs) are van der Waals materials that hold great promise for nanoscale optoelectronics thanks to their strong light−matter interactions even at the atomically thin limit. The optoelectronic properties of 2D TMDs are in large part governed by their Coulomb-bound electron−hole pairs (excitons) with relatively large binding energies of up to hundreds of millielectronvolts (meV) due to weak out-of-plane dielectric screening.[1−6] Unlike free charges, excitons are charge neutral and are therefore difficult to manipulate with external electric fields in electronic devices.[7−9] Therefore, the transport properties of excitons are largely dictated by random, diffusive motion with no long-range directionality, limiting their use as information and energy carriers. Finding new ways to manipulate exciton transport in 2D TMDs without radically altering other material properties would result in excitonic devices that combine strong light−matter interactions and precise control over energy and information flow in atomically thin materials.

An attractive route to controlling the properties of 2D TMDs is to leverage their extreme sensitivity to extrinsic factors such as strain,[10−21] and dielectric screening by the environment (Figure 1a),[5,22−26] enabling postsynthetic tuning of their optoelectronic and transport properties. For example, tensile strain reduces the optical transition energy of 2D TMDs;[16,18,27,28] localized strain regions thus create energy gradients that can funnel and trap excitons in nanoscale low-energy sites, a process that was leveraged to create long-lived quantum emitters.[14,29−33] Strain engineering, however, is difficult to control over macroscopic scales and can introduce undesired disorder.

A less invasive and in principle more controlled approach is to modulate Coulomb interactions in 2D TMDs through dielectric engineering of the surrounding environment, for example, by modifying the substrate on which TMD layers are deposited.[22] The dielectric contrast at the interface of monolayer or few-layer TMDs leads to extreme sensitivity of their Coulomb interactions to the environment.[2,6,22,34,35] Although dielectric engineering has indeed been used to successfully modulate some TMD properties, changes in absorption and photoluminescence energies (the optical gap $E_{opt}$) of 2D TMDs as a function of substrate dielectric constant are predicted to be surprisingly small: ∼100 meV for a 20-fold increase in substrate dielectric constant.[36] These modest changes arise from a cancellation effect between a large dielectric-induced change of the single-particle bandgap ($\Delta E_g$, the minimum gap between the conduction and valence bands without electron−hole correlations) and a similarly large change in the exciton binding energy ($\Delta E_b$),[36] which overall results in small changes to $\Delta E_{opt} = \Delta E_g - \Delta E_b$ (using positive binding energies as convention), as depicted in Figure 1b.

**Received:** December 27, 2021
**Revised:** March 8, 2022
**Published:** March 16, 2022

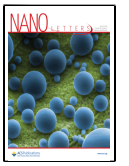





https://doi.org/10.1021/acs.nanolett.1c04997
*Nano Lett.* 2022, 22, 2843−2850

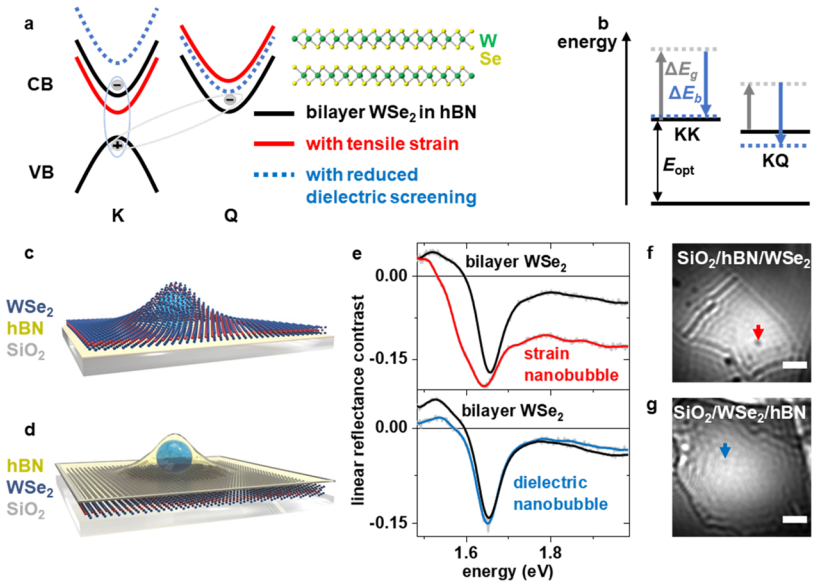


**Figure 1.** (a) Schematic single-particle valence and conduction bands (energy vs momentum) for bilayer $WSe_2$ at the $K$ and $Q$ (often labeled $\Lambda$) valleys, showing bright KK momentum-direct excitons and dark KQ momentum-indirect excitons. Spin-forbidden dark states are ignored. The proposed effects of tensile strain and reduced dielectric screening on the single-particle bands are illustrated in red and blue, respectively. (b) Exciton energy-level diagram displaying the effect of reduced dielectric screening on the single-particle bandgap ($\Delta E_g$) and binding energy ($\Delta E_b$) in gray and blue arrows, respectively. (c,d) Illustrations of a strain nanobubble (c) and a dielectric nanobubble (d). (e) Linear reflectance contrast, $(R_{sample} - R_{substrate})/R_{substrate}$ obtained with an oil-immersion objective for flat regions of bilayer $WSe_2$ (black), strain nanobubbles (red), and dielectric nanobubbles (blue). (f,g) iSCAT images taken at a probe wavelength of 1.62 eV for samples containing strain nanobubbles (f) and dielectric nanobubbles (g). The arrows point to two example nanobubbles; strain nanobubbles are clearly visible, whereas dielectric nanobubbles are barely distinguishable. Scale bars are 2 $\mu$m.

Although this weak dependence of $E_{opt}$ on the dielectric environment limits the applicability of dielectric engineering for bright, momentum-direct (KK) excitons, 2D TMDs also sustain a wealth of intervalley, momentum-indirect "dark" excitons (e.g., KQ and ΓQ excitons, illustrated in Figure 1a for the $K$ and $Q$ valleys) for which the viability of dielectric engineering remains unexplored. Since dielectric insensitivity for KK excitons results from the near cancellation of two large contributions, small differences in either $\Delta E_g$ or $\Delta E_b$ could substantially enhance the environmental sensitivity of other excitons. For example, recent calculations suggest that dielectric-induced $\Delta E_g$ at the $Q$ valley is substantially smaller than at the $K$ valley[37] (Figure 1a). This modification would prevent a full cancellation effect with $\Delta E_b$, resulting in a much larger environmental sensitivity for KQ excitons compared to KK excitons (Figure 1b). Nevertheless, dark excitons cannot be directly probed by absorption or photoluminescence at room temperature,[38−44] creating a significant obstacle to confirming and leveraging the environmental sensitivity of a large population of excitons in TMDs.

In this work, we show that dark excitons exhibit a greater sensitivity to their dielectric environment with reduced energies in the presence of reduced dielectric screening (Figure 1b), enabling dielectrically engineered exciton transport. We use spatiotemporally resolved optical scattering microscopy[45] to directly image the transport of the total population of excitons in heterogeneous dielectric environments at room temperature. We study bilayer $WSe_2$ because it hosts a number of momentum-dark excitons that lie tens to hundreds of millielectronvolts lower in energy than the bright KK exciton, ensuring that the majority of excitons populate momentum-indirect states at room temperature.[32,39,41,46] We reveal that excitons can be efficiently funneled into nanoscale dielectric inhomogeneities even though the energies of bright excitons are negligibly affected, from which we draw conclusions about the environmental sensitivity of dark excitons. Leveraging the important contribution of dark excitons and their large dependence on environmental dielectric represents a new approach for highly effective, noninvasive manipulation of exciton transport and dynamics in TMDs.

To manipulate excitons and concentrate them into spatially well-defined regions at room temperature, we use bilayer 2H-$WSe_2$/hexagonal boron nitride (hBN) heterostructures containing nanobubbles. Nanobubbles are nanoscale regions of trapped adsorbates that form naturally between mechanically stacked van der Waals layers in heterostructures.[47−50] In our heterostructures, the nanobubbles create regions of strain either in $WSe_2$ or in hBN, as illustrated in Figure 1c,d, respectively. We control the type of nanobubbles formed through the stacking order (Supporting Information Section 1). "Strain nanobubbles" occur when the $WSe_2$ is strained, leading to the well-known strain-induced modulation of exciton energies[50,51] (Figure 1a). In contrast, the nanobubbles formed in hBN create nanoscale regions of slightly lower dielectric screening wherever the hBN and $WSe_2$ are not in contact without directly affecting the $WSe_2$. We term these regions "dielectric nanobubbles". Our structures therefore allow direct comparison between the effect of strain and dielectric inhomogeneities on exciton transport. The bilayers are mechanically exfoliated from ultrapure flux-grown crystals[52,53] that minimize the influence of intrinsic defects on exciton dynamics, providing confidence in our assignment of strain and dielectric effects on exciton transport.

Figure 1e shows the linear, room-temperature reflectance contrast spectra near the A-exciton (bright KK) resonance for


https://doi.org/10.1021/acs.nanolett.1c04997
Nano Lett. 2022, 22, 2843−2850

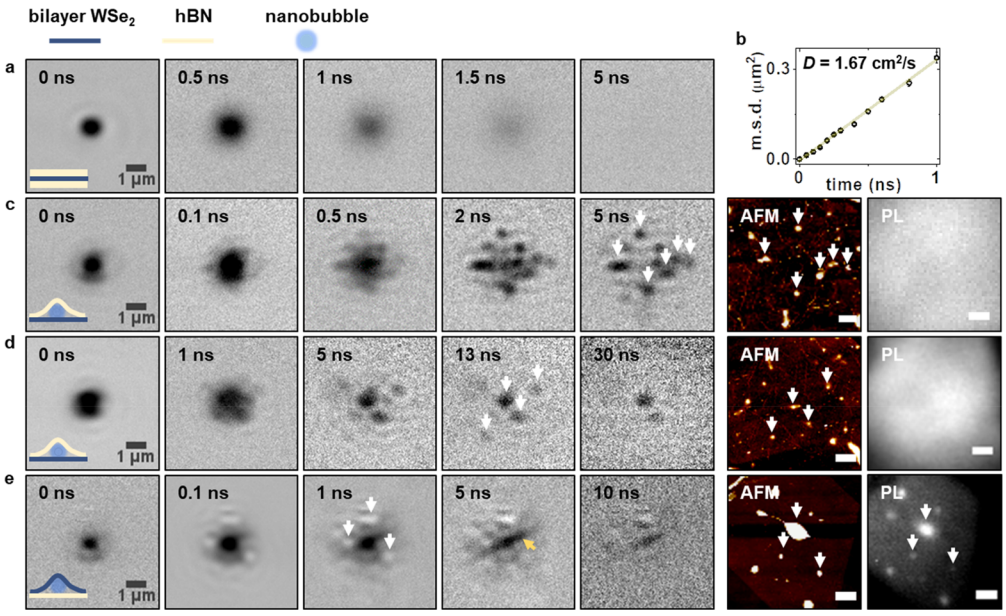


**Figure 2.** (a) stroboSCAT images of exciton transport in fully encapsulated bilayer $WSe_2$. (b) Mean-squared displacement (m.s.d.) for the data shown in panel (a). The line is a linear fit to the data (circles), providing a diffusion coefficient $D$ = 1.67 $cm^2/s$ for excitons in encapsulated bilayer $WSe_2$. (c,d) stroboSCAT, AFM and PL images for bilayer $WSe_2$/hBN heterostructures in regions with dielectric nanobubbles. We observe clear exciton localization with stroboSCAT, at locations that correlate with AFM images of the nanobubbles, as indicated by white arrows; PL images (taken with widefield illumination using a 1.9 eV laser), however, do not show any evidence of exciton localization. (e) stroboSCAT, AFM, and PL images for a bilayer $WSe_2$/hBN heterostructure in a region with strain nanobubbles. Excitons localizing in strain nanobubbles switch to bright contrast, and correlate with both AFM and PL images. Additional features (e.g., gold arrow) indicate a disordered energetic landscape, as detailed in the text. For all stroboSCAT data sets, pump and probe wavelengths are 2.82 and 1.62 eV, respectively. The pump fluence is ∼150 $nJ/cm^2$, corresponding to ∼10 excitons per diffraction-limited spot which avoids trap saturation effects that occur at higher pump fluences. All scale bars are 1 $\mu$m.

$WSe_2$ at strain and dielectric nanobubbles compared to nearby flat regions. The strain nanobubble exhibits a broader spectrum and a redshift of ∼65 meV compared to the flat region. In contrast, the $WSe_2$ spectrum changes negligibly at the location of dielectric nanobubbles, suggesting that single-side hBN encapsulation of glass-supported bilayer $WSe_2$ barely influences the optical gap. Both of these observations are consistent with previous reports.[22,50] In Figure 1f,g, we display interferometric scattering microscopy (iSCAT) images of the two types of heterostructures. iSCAT is an extremely sensitive version of brightfield reflectance microscopy.[54−56] Strain nanobubbles are clearly visible in iSCAT, similarly to brightfield microscopy; dielectric nanobubbles, however, are barely distinguishable in iSCAT and invisible in brightfield microscopy. As such, although nanobubbles form regularly in van der Waals heterostructures (as observed for example in AFM images, *vide infra*), they can be easily overlooked if they only strain transparent screening layers.

To determine the effect of nanobubbles on exciton transport, we turn to a pump−probe version of iSCAT, stroboscopic scattering microscopy (stroboSCAT).[45] stroboSCAT is a spatiotemporally resolved far-field imaging approach[57,58] wherein a diffraction-limited optical excitation generates a population of excitons, and a widefield backscattering optical probe images the spatial distribution of photogenerated excitons at controllable time delays later (Figure S2). These measurements directly track the motion of excitons in real space with picosecond resolution and few-nanometer precision. Contrast in stroboSCAT is generated by pump-induced changes to material polarizability,[45,59,60] and is thus sensitive to species such as momentum-dark excitons because their presence modifies the polarizability of optically allowed transitions, even if there is no direct population exchange between dark and bright excitons. In contrast, photoluminescence (PL), a powerful contrast mechanism often used for spatiotemporal imaging of exciton transport in TMDs,[61−63] requires population transfer from dark to bright states followed by recombination through momentum-allowed channels, or alternative brightening mechanisms, to be sensitive to momentum-dark excitons at room temperature. We show below that these differences in contrast generation give rise to important discrepancies between stroboSCAT and PL images and uniquely enable stroboSCAT to monitor momentum-dark excitons trapped in deep potential wells. To perform the experiments described below in the linear regime (without exciton trap saturation), pump excitation fluences are limited to the generation of ∼10 excitons per diffraction-limited spot. We achieve the necessary sensitivity for probing such low exciton densities by tuning our probe energy slightly lower than the optical gap, operating in a preresonance regime that dramatically enhances backscattering contrast without perturbing the sample (Supporting Information Section 2).

Figure 2a displays stroboSCAT images taken on bilayer $WSe_2$ encapsulated on both sides by hBN. The expanding dark contrast corresponds to diffusing pump-generated excitons. Full hBN encapsulation is known to considerably reduce the effect of dielectric disorder on exciton dynamics.[34,64−66] Indeed, our measurements on fully encapsulated $WSe_2$ indicate that even if nanobubbles are present in the top hBN layer, effective dielectric screening is still provided by the bottom layer. As a result, the exciton dynamics in $WSe_2$ are virtually oblivious to nanobubbles, in stark contrast to the half-


https://doi.org/10.1021/acs.nanolett.1c04997
Nano Lett. 2022, 22, 2843−2850

encapsulated samples described below. Thus, in fully encapsulated samples, we observe perfectly isotropic and diffusive exciton transport. From the mean-squared displacement (m.s.d.) of the exciton population, $\sigma^2(t) - \sigma^2(0) = 2Dt$ (Supporting Information Section 1.3), where $\sigma(t)$ is the Gaussian width of the exciton spatial distribution at pump−probe time delay $t$, we extract an intrinsic diffusivity $D = 1.67 \pm 0.03$ cm$^2$/s (Figure 2b) for excitons in encapsulated bilayer $WSe_2$. We observe similar diffusivities in nanobubble-free regions of top-encapsulated structures (glass/bilayer $WSe_2$/hBN), but 3-fold lower diffusivities in nonencapsulated bilayer $WSe_2$ (Figure S4), suggesting that hBN encapsulation enhances exciton transport thanks to suppressed disorder, in agreement with prior observations in monolayer TMDs.[66]

Our key results are displayed in Figures 2c,d which show two examples of exciton dynamics in single-side encapsulated samples in the presence of dielectric nanobubbles. We observe visually striking evidence of excitons localizing at nanoscale sites on nanosecond time scales after which the excitons stop migrating and remain in some cases for over 30 ns. We confirm that the trap locations (highlighted with white arrows) are nanobubbles by spatially correlating the stroboSCAT images to atomic force microscopy images (AFM, middle-right panel). The AFM images show ∼5−30 nm tall topographical features that are characteristic of nanobubbles. The locations of these nanobubbles correspond precisely to the exciton localization identified in stroboSCAT. Conversely, PL images (right panels) exhibit subtle micron-scale inhomogeneities, as observed in other studies of dielectric disorder,[34] but remarkably do not display any evidence of the presence of nanobubbles. This lack of correspondence between PL images and stroboSCAT is a strong indication that the observed exciton dynamics in bilayer $WSe_2$ are not governed by bright, emissive states; instead, exciton localization in dielectric nanobubbles is likely driven by momentum-dark (KQ) excitons, which dominate the exciton population in bilayer $WSe_2$.

To further elucidate the role of momentum-dark excitons in these surprising observations, we performed stroboSCAT measurements on monolayer $WSe_2$/hBN heterostructures. KK and KQ excitons are almost isoenergetic in monolayer $WSe_2$, and a large fraction of the total exciton population is bright at room temperature.[39,46,67] We expect bright excitons to be oblivious to or slightly repelled by dielectric nanobubbles, because the lower dielectric screening in these regions should raise the KK energy by ∼20 meV.[22,36] Our results indeed indicate that dielectric nanobubbles only subtly perturb exciton transport dynamics in monolayer $WSe_2$, and we find no evidence of long-lived exciton localization in the nanobubbles (Figure S5). These results lend further support to our hypothesis that momentum-indirect states govern exciton dynamics in bilayer $WSe_2$ and are responsible for the dramatic modification of exciton transport properties in the presence of dielectric inhomogeneities.

To compare the effects of dielectric engineering with the more commonly encountered strain engineering, we now turn to bilayer $WSe_2$/hBN heterostructures containing strain nanobubbles (Figure 2e). Tensile strain in the nanobubbles causes the optical gap of $WSe_2$ to be lowered by several tens of millielectronvolts compared to surrounding unstrained regions (Figure 1e) and raises the KQ exciton energies by a similar amount (Figure 1a).[32,39,51,68,69] We observe exciton localization in these nanobubbles (indicated by white arrows, spatially correlated to AFM images) but with several important differences compared to the dielectric nanobubbles of Figures 2c,d. First, the stroboSCAT signal for the trapped excitons in strain nanobubbles is inverted, showing bright rather than dark contrast. This behavior is expected in preresonant stroboSCAT when probing optically accessible lower-energy sites (Supporting Information Section 2). Second, we observe significantly enhanced PL at these nanobubbles (Figure 2e, right panel) which is in agreement with previous reports.[49,50] Together, these results confirm that exciton dynamics within strain nanobubbles in bilayer $WSe_2$ are governed by bright KK excitons. Indeed, our measured strain-induced redshift of ∼65 meV implies an average strain of 1.25% at the nanobubble location,[70] well within the range of predicted strain-induced switching from momentum-indirect to direct bandgap character in bilayer $WSe_2$.[16,32,39] The clear differences observed between dielectric and strain nanobubbles also confirm that the modulation of exciton dynamics in dielectric nanobubbles occurs through a different mechanism than semiconductor strain.

Finally, the stroboSCAT images of Figure 2e indicate a strongly disordered landscape with localization and long-lived states appearing not just in nanobubbles but also in other inhomogeneities not observed in the PL image. For example, the gold arrow in Figure 2e highlights a long-lived, linelike feature with dark contrast appearing between nanobubbles. This feature may arise from regions of compressive strain between closely spaced nanobubbles, which carries an opposite effect to tensile strain (raised KK and lowered KQ exciton energies)[39,68,69] and could lead to dark-state trapping that would explain the absence of this feature in the PL image. Similarly, recent work suggests that momentum-dark excitons experience antifunneling (i.e., move away) from tensile strain regions,[71] which may explain our observation of trapped momentum-indirect excitons between closely spaced strain nanobubbles.

To provide further insight into how dielectric nanobubbles modify exciton transport, Figure 3a displays the dynamics of excitons taken from the data in Figure 2d, demonstrating that the lifetime of excitons trapped in dielectric nanobubbles is dramatically prolonged. For example, for the nanobubble at the top-right of the excitation spot in Figure 2d we extract a lifetime of 12 ns (blue curve in Figure 3a), a 26-fold increase over the lifetime of excitons in flat regions of the bilayer $WSe_2$/hBN heterostructures. Assuming the lifetime is dictated by thermally activated detrapping from the low-energy sites in the nanobubble and ignoring entropic contributions, a 26-fold lifetime enhancement suggests that an 84 meV deep trap is formed by dielectric nanobubbles. Strain nanobubbles lead to more modest exciton lifetime enhancements (Figure S6) in our heterostructures which is an unsurprising finding since the bright states in strain nanobubbles relax through momentum-allowed channels, in contrast to the detrapping and intervalley scattering required for the relaxation of momentum-dark excitons trapped in dielectric nanobubbles.

Comparing the observed rise-time of the signal at dielectric nanobubbles with the expected rise time calculated from the known diffusivity of 1.67 cm$^2$/s (gray trace in Figure 3a), we find that excitons reach the nanobubbles more than twice as fast as would be expected in a purely diffusive model (time of maximum population is 2.2 ns instead of the expected 4.7 ns). These results indicate that downhill energy gradients caused by dielectric nanobubbles cause directional funneling of excitons


https://doi.org/10.1021/acs.nanolett.1c04997
Nano Lett. 2022, 22, 2843−2850

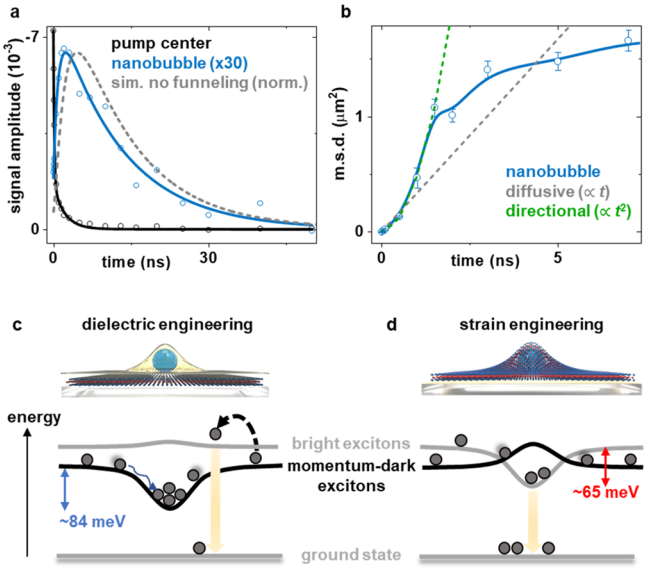


**Figure 3.** (a) Exciton dynamics in dielectric nanobubbles (from stroboSCAT data in Figure 2d). The lines are biexponential fits to the data that we use to extract the lifetime of trapped excitons. The gray trace is calculated from an isotropic diffusion model with $D$ = 1.67 $cm^2/s$, showing that excitons funnel into nanobubbles faster than expected from a purely diffusive model. (b) Mean-squared displacement (m.s.d.) obtained for exciton transport toward a nanobubble for the data in Figure S7 and Movie S1 (blue data in open circles, with a spline curve to guide the eye). The m.s.d. toward the nanobubble exceeds that expected for purely diffusive transport with $D$ = 1.67 $cm^2/s$ (gray trace). A superdiffusive fit (green trace) to the early time data suggests the m.s.d. is initially proportional to $t^2$, indicating funneling into nanobubbles. (c,d) Summary energy-level diagrams illustrating exciton dynamics in bilayer $WSe_2$/hBN heterostructures in the presence of dielectric (c) and strain (d) nanobubbles. The quoted trapping energies are representative numbers extracted from data sets presented in the text but can vary from site to site. Black dashed arrows indicate thermally activated detrapping or intervalley scattering, while yellow arrows indicate radiative recombination.

toward the nanobubbles. Exciton funneling is visually most evident in stroboSCAT movies of exciton migration in samples with just a few nanobubbles (Movies S1 and S2). Figure 3b plots the m.s.d. for exciton transport into a nanobubble from the data in Movie S1 (analysis in Figure S7). For purely random, diffusive behavior, we expect the m.s.d. to be proportional to time, as indicated in the gray dashed trace in Figure 3b for $D$ = 1.67 $cm^2/s$. Instead, exciton transport toward the nanobubble is superdiffusive. We extract an m.s.d. proportional to $t^2$ prior to the excitons trapping in the nanobubble (the green trace in Figure 3b is a superdiffusive fit to the first five blue data points). This behavior indicates directional transport (drift) of excitons into the nanobubble due to a progressive downhill energy gradient created by the dielectric perturbation of the nanobubble. Our data imply a drift velocity of 640 nm/ns sustained over a distance of 1 $\mu$m, similar to the exciton drift velocities and distances achieved using large strain gradients in monolayer TMDs[13,63] and in close agreement with our drift-diffusion simulations for this sample (Figure S7). These results provide additional confirmation that excitons are indeed efficiently funneled, rather than simply trapped, by dielectric inhomogeneities, providing a pathway to manipulating exciton transport with high precision over macroscopic scales and to concentrate excitons in target regions with nanoscale precision.

Overall, our results indicate that dielectric engineering is particularly effective for TMDs in which the majority of excitons reside in low-lying momentum-indirect states. Leveraging this effect, we show that nanobubbles in a hBN dielectric screening layer provides an efficient path to controlling exciton dynamics in bilayer $WSe_2$. As summarized in Figures 3c,d, the use of nanobubbles allows a direct comparison of tensile strain and dielectric engineering. Tensile strain allows funneling of bright excitons into bright states which is advantageous for emitter-based functions. Dielectric engineering, however, is less invasive and achieves longer exciton lifetimes through momentum-dark excitons that are valuable for light harvesting and information processing applications. Our experimentally observed dependence of momentum-indirect excitons on their dielectric environment is consistent with their larger effective mass and therefore larger binding energy renormalization than KK excitons,[38−40,72] combined with a reduced sensitivity in their band gap. The latter has been observed in a recent GW calculation of monolayer $MoS_2$,[37] although it was not observed in a similar previous calculation on monolayer $WS_2$.[73] Resolving these small energy differences due to dielectric effects is an ongoing challenge for theoretical calculations.

We anticipate that patterning of high-dielectric substrates such as graphite[22] on which bilayer TMDs are deposited will provide a platform to predictively manipulate exciton transport with high precision for new, dark-exciton driven functionalities in nanoscale devices. The combination of efficient funneling and long lifetimes of momentum-dark excitons in dielectric inhomogeneities could be leveraged to drive spatially confined population inversion, as well as to concentrate excitons generated across macroscopic areas into nanoscale catalytically active regions to drive photocatalysis under low-light conditions, a strategy similar to exciton funneling from light harvesting antennae into reaction centers in photosynthetic organisms.

## ■ ASSOCIATED CONTENT

### Supporting Information

The Supporting Information is available free of charge at https://pubs.acs.org/doi/10.1021/acs.nanolett.1c04997.

Materials and methods (Figures S1, S2), details of preresonant stroboSCAT contrast mechanism (Figure S3), and additional data (Figures S4−S7) (PDF)

Movie S1: Funneling in dielectric nanobubbles (1) (AVI)

Movie S2: Funneling in dielectric nanobubbles (2) (AVI)

## ■ AUTHOR INFORMATION


### Corresponding Author

**Milan Delor** − *Department of Chemistry, Columbia University, New York, New York 10027, United States;* orcid.org/0000-0002-9480-9235; Email: milan.delor@columbia.edu

### Authors

**Haowen Su** − *Department of Chemistry, Columbia University, New York, New York 10027, United States*




https://doi.org/10.1021/acs.nanolett.1c04997
*Nano Lett.* 2022, 22, 2843−2850

**Ding Xu** − *Department of Chemistry, Columbia University, New York, New York 10027, United States*
**Shan-Wen Cheng** − *Department of Chemistry, Columbia University, New York, New York 10027, United States*
**Baichang Li** − *Department of Mechanical Engineering, Columbia University, New York, New York 10027, United States;* orcid.org/0000-0002-2345-6735
**Song Liu** − *Department of Mechanical Engineering, Columbia University, New York, New York 10027, United States*
**Kenji Watanabe** − *Research Center for Functional Materials, National Institute for Materials Science, Tsukuba, Ibaraki 305-0044, Japan;* orcid.org/0000-0003-3701-8119
**Takashi Taniguchi** − *International Center for Materials Nanoarchitectonics, National Institute for Materials Science, Tsukuba, Ibaraki 305-0044, Japan;* orcid.org/0000-0002-1467-3105
**Timothy C. Berkelbach** − *Department of Chemistry, Columbia University, New York, New York 10027, United States; Center for Computational Quantum Physics, Flatiron Institute, New York, New York 10010, United States*
**James C. Hone** − *Department of Mechanical Engineering, Columbia University, New York, New York 10027, United States*

Complete contact information is available at: https://pubs.acs.org/10.1021/acs.nanolett.1c04997

### Notes

The authors declare no competing financial interest.

## ■ ACKNOWLEDGMENTS

We thank Thomas P. Darlington and Professor P. James Schuck (Columbia University) for helpful discussions. This material is based upon work supported by the National Science Foundation under Grant DMR-2115625. Synthesis of $WSe_2$ (S.L. and J.H.) was supported by the NSF MRSEC program through Columbia in the Center for Precision-Assembled Quantum Materials (DMR-2011738). Synthesis of hBN (K.W. and T.T.) was supported by the Elemental Strategy Initiative conducted by the MEXT, Japan (Grant JPMXP0112101001), and JSPS KAKENHI (Grants JP19H05790 and JP20H00354). The Flatiron Institute is a division of the Simons Foundation.

## ■ REFERENCES

(1) Mak, K. F.; Lee, C.; Hone, J.; Shan, J.; Heinz, T. F. Atomically Thin $MoS_2$: A New Direct-Gap Semiconductor. *Phys. Rev. Lett.* **2010**, *105*, 136805.
(2) Wang, G.; Chernikov, A.; Glazov, M. M.; Heinz, T. F.; Marie, X.; Amand, T.; Urbaszek, B. Colloquium : Excitons in Atomically Thin Transition Metal Dichalcogenides. *Rev. Mod. Phys.* **2018**, *90*, 021001.
(3) Mueller, T.; Malic, E. Exciton Physics and Device Application of Two-Dimensional Transition Metal Dichalcogenide Semiconductors. *npj 2D Mater. Appl.* **2018**, *2*, 29.
(4) Kylänpää, I.; Komsa, H.-P. Binding Energies of Exciton Complexes in Transition Metal Dichalcogenide Monolayers and Effect of Dielectric Environment. *Phys. Rev. B* **2015**, *92*, 205418.
(5) Latini, S.; Olsen, T.; Thygesen, K. S. Excitons in van Der Waals Heterostructures: The Important Role of Dielectric Screening. *Phys. Rev. B - Condens. Matter Mater. Phys.* **2015**, *92*, 245123.
(6) Berkelbach, T. C.; Reichman, D. R. Optical and Excitonic Properties of Atomically Thin Transition-Metal Dichalcogenides. *Annu. Rev. Condens. Matter Phys.* **2018**, *9*, 379−396.
(7) High, A. A.; Novitskaya, E. E.; Butov, L. V.; Hanson, M.; Gossard, A. C. Control of Exciton Fluxes in an Excitonic Integrated Circuit. *Science* **2008**, *321*, 229−231.
(8) Unuchek, D.; Ciarrocchi, A.; Avsar, A.; Watanabe, K.; Taniguchi, T.; Kis, A. Room-Temperature Electrical Control of Exciton Flux in a van Der Waals Heterostructure. *Nature* **2018**, *560*, 340−344.
(9) Jauregui, L. A.; Joe, A. Y.; Pistunova, K.; Wild, D. S.; High, A. A.; Zhou, Y.; Scuri, G.; De Greve, K.; Sushko, A.; Yu, C.-H.; Taniguchi, T.; Watanabe, K.; Needleman, D. J.; Lukin, M. D.; Park, H.; Kim, P. Electrical Control of Interlayer Exciton Dynamics in Atomically Thin Heterostructures. *Science* **2019**, *366*, 870−875.
(10) Johari, P.; Shenoy, V. B. Tuning the Electronic Properties of Semiconducting Transition Metal Dichalcogenides by Applying Mechanical Strains. *ACS Nano* **2012**, *6*, 5449−5456.
(11) Castellanos-Gomez, A.; Roldán, R.; Cappelluti, E.; Buscema, M.; Guinea, F.; van der Zant, H. S. J.; Steele, G. A. Local Strain Engineering in Atomically Thin $MoS_2$. *Nano Lett.* **2013**, *13*, 5361−5366.
(12) Li, H.; Contryman, A. W.; Qian, X.; Ardakani, S. M.; Gong, Y.; Wang, X.; Weisse, J. M.; Lee, C. H.; Zhao, J.; Ajayan, P. M.; Li, J.; Manoharan, H. C.; Zheng, X. Optoelectronic Crystal of Artificial Atoms in Strain-Textured Molybdenum Disulphide. *Nat. Commun.* **2015**, *6*, 7381.
(13) Moon, H.; Grosso, G.; Chakraborty, C.; Peng, C.; Taniguchi, T.; Watanabe, K.; Englund, D. Dynamic Exciton Funneling by Local Strain Control in a Monolayer Semiconductor. *Nano Lett.* **2020**, *20*, 6791−6797.
(14) Conley, H. J.; Wang, B.; Ziegler, J. I.; Haglund, R. F.; Pantelides, S. T.; Bolotin, K. I. Bandgap Engineering of Strained Monolayer and Bilayer $MoS_2$. *Nano Lett.* **2013**, *13*, 3626−3630.
(15) Lloyd, D.; Liu, X.; Christopher, J. W.; Cantley, L.; Wadehra, A.; Kim, B. L.; Goldberg, B. B.; Swan, A. K.; Bunch, J. S. Band Gap Engineering with Ultralarge Biaxial Strains in Suspended Monolayer $MoS_2$. *Nano Lett.* **2016**, *16*, 5836−5841.
(16) Desai, S. B.; Seol, G.; Kang, J. S.; Fang, H.; Battaglia, C.; Kapadia, R.; Ager, J. W.; Guo, J.; Javey, A. Strain-Induced Indirect to Direct Bandgap Transition in Multilayer $WSe_2$. *Nano Lett.* **2014**, *14*, 4592−4597.
(17) Niehues, I.; Schmidt, R.; Drüppel, M.; Marauhn, P.; Christiansen, D.; Selig, M.; Berghäuser, G.; Wigger, D.; Schneider, R.; Braasch, L.; Koch, R.; Castellanos-Gomez, A.; Kuhn, T.; Knorr, A.; Malic, E.; Rohlfing, M.; Michaelis de Vasconcellos, S.; Bratschitsch, R. Strain Control of Exciton−Phonon Coupling in Atomically Thin Semiconductors. *Nano Lett.* **2018**, *18*, 1751−1757.
(18) Feng, J.; Qian, X.; Huang, C.-W.; Li, J. Strain-Engineered Artificial Atom as a Broad-Spectrum Solar Energy Funnel. *Nat. Photonics* **2012**, *6*, 866−872.
(19) Yan, Y.; Ding, S.; Wu, X.; Zhu, J.; Feng, D.; Yang, X.; Li, F. Tuning the Physical Properties of Ultrathin Transition-Metal Dichalcogenides via Strain Engineering. *RSC Adv.* **2020**, *10*, 39455−39467.
(20) Xie, S.; Tu, L.; Han, Y.; Huang, L.; Kang, K.; Lao, K. U.; Poddar, P.; Park, C.; Muller, D. A.; DiStasio, R. A.; Park, J. Coherent, Atomically Thin Transition-Metal Dichalcogenide Superlattices with Engineered Strain. *Science* **2018**, *359*, 1131−1136.
(21) Branny, A.; Kumar, S.; Proux, R.; Gerardot, B. D Deterministic Strain-Induced Arrays of Quantum Emitters in a Two-Dimensional Semiconductor. *Nat. Commun.* **2017**, *8*, 15053.
(22) Raja, A.; Chaves, A.; Yu, J.; Arefe, G.; Hill, H. M.; Rigosi, A. F.; Berkelbach, T. C.; Nagler, P.; Schüller, C.; Korn, T.; Nuckolls, C.; Hone, J.; Brus, L. E.; Heinz, T. F.; Reichman, D. R.; Chernikov, A. Coulomb Engineering of the Bandgap and Excitons in Two-Dimensional Materials. *Nat. Commun.* **2017**, *8*, 15251.
(23) Steinke, C.; Mourad, D.; Rösner, M.; Lorke, M.; Gies, C.; Jahnke, F.; Czycholl, G.; Wehling, T. O. Noninvasive Control of Excitons in Two-Dimensional Materials. *Phys. Rev. B* **2017**, *96*, 045431.
(24) Borghardt, S.; Tu, J.-S.; Winkler, F.; Schubert, J.; Zander, W.; Leosson, K.; Kardynał, B. E. Engineering of Optical and Electronic Band Gaps in Transition Metal Dichalcogenide Monolayers through External Dielectric Screening. *Phys. Rev. Mater.* **2017**, *1*, 054001.

(25) Yu, Y.; Yu, Y.; Xu, C.; Cai, Y.-Q.; Su, L.; Zhang, Y.; Zhang, Y.-W.; Gundogdu, K.; Cao, L. Engineering Substrate Interactions for High Luminescence Efficiency of Transition-Metal Dichalcogenide Monolayers. *Adv. Funct. Mater.* **2016**, *26*, 4733−4739.
(26) Li, Z.; Cordovilla Leon, D. F.; Lee, W.; Datta, K.; Lyu, Z.; Hou, J.; Taniguchi, T.; Watanabe, K.; Kioupakis, E.; Deotare, P. B. Dielectric Engineering for Manipulating Exciton Transport in Semiconductor Monolayers. *Nano Lett.* **2021**, *21*, 8409−8417.
(27) Roldán, R.; Castellanos-Gomez, A.; Cappelluti, E.; Guinea, F. Strain Engineering in Semiconducting Two-Dimensional Crystals. *J. Phys.: Condens. Matter* **2015**, *27*, 313201.
(28) Defo, R. K.; Fang, S.; Shirodkar, S. N.; Tritsaris, G. A.; Dimoulas, A.; Kaxiras, E. Strain Dependence of Band Gaps and Exciton Energies in Pure and Mixed Transition-Metal Dichalcogenides. *Phys. Rev. B* **2016**, *94*, 155310.
(29) Luo, Y.; Shepard, G. D.; Ardelean, J. V.; Rhodes, D. A.; Kim, B.; Barmak, K.; Hone, J. C.; Strauf, S. Deterministic Coupling of Site-Controlled Quantum Emitters in Monolayer $WSe_2$ to Plasmonic Nanocavities. *Nat. Nanotechnol.* **2018**, *13*, 1137−1142.
(30) Shepard, G. D.; Ajayi, O. A.; Li, X.; Zhu, X.-Y.; Hone, J.; Strauf, S. Nanobubble Induced Formation of Quantum Emitters in Monolayer Semiconductors. *2D Mater.* **2017**, *4*, 021019.
(31) Amin, B.; Kaloni, T. P.; Schwingenschlögl, U. Strain Engineering of $WS_2$, $WSe_2$, and $WTe_2$. *RSC Adv.* **2014**, *4*, 34561−34565.
(32) Aslan, O. B.; Deng, M.; Brongersma, M. L.; Heinz, T. F. Strained Bilayer $WSe_2$ with Reduced Exciton-Phonon Coupling. *Phys. Rev. B* **2020**, *101*, 115305.
(33) Tonndorf, P.; Schmidt, R.; Schneider, R.; Kern, J.; Buscema, M.; Steele, G. A.; Castellanos-Gomez, A.; van der Zant, H. S. J.; Michaelis de Vasconcellos, S.; Bratschitsch, R. Single-Photon Emission from Localized Excitons in an Atomically Thin Semiconductor. *Optica* **2015**, *2*, 347.
(34) Raja, A.; Waldecker, L.; Zipfel, J.; Cho, Y.; Brem, S.; Ziegler, J. D.; Kulig, M.; Taniguchi, T.; Watanabe, K.; Malic, E.; Heinz, T. F.; Berkelbach, T. C.; Chernikov, A. Dielectric Disorder in Two-Dimensional Materials. *Nat. Nanotechnol.* **2019**, *14*, 832−837.
(35) Chernikov, A.; Berkelbach, T. C.; Hill, H. M.; Rigosi, A.; Li, Y.; Aslan, O. B.; Reichman, D. R.; Hybertsen, M. S.; Heinz, T. F. Exciton Binding Energy and Nonhydrogenic Rydberg Series in Monolayer $WS_2$. *Phys. Rev. Lett.* **2014**, *113*, 076802.
(36) Cho, Y.; Berkelbach, T. C. Environmentally Sensitive Theory of Electronic and Optical Transitions in Atomically Thin Semiconductors. *Phys. Rev. B* **2018**, *97*, 041409.
(37) Zibouche, N.; Schlipf, M.; Giustino, F. GW Band Structure of Monolayer $MoS_2$ Using the SternheimerGW Method and Effect of Dielectric Environment. *Phys. Rev. B* **2021**, *103*, 125401.
(38) Malic, E.; Selig, M.; Feierabend, M.; Brem, S.; Christiansen, D.; Wendler, F.; Knorr, A.; Berghäuser, G. Dark Excitons in Transition Metal Dichalcogenides. *Phys. Rev. Mater.* **2018**, *2*, 014002.
(39) Deilmann, T.; Thygesen, K. S. Finite-Momentum Exciton Landscape in Mono- and Bilayer Transition Metal Dichalcogenides. *2D Mater.* **2019**, *6*, 035003.
(40) Brem, S.; Ekman, A.; Christiansen, D.; Katsch, F.; Selig, M.; Robert, C.; Marie, X.; Urbaszek, B.; Knorr, A.; Malic, E. Phonon-Assisted Photoluminescence from Indirect Excitons in Monolayers of Transition-Metal Dichalcogenides. *Nano Lett.* **2020**, *20*, 2849−2856.
(41) Lindlau, J.; Selig, M.; Neumann, A.; Colombier, L.; Förste, J.; Funk, V.; Förg, M.; Kim, J.; Berghäuser, G.; Taniguchi, T.; Watanabe, K.; Wang, F.; Malic, E.; Högele, A. The Role of Momentum-Dark Excitons in the Elementary Optical Response of Bilayer $WSe_2$. *Nat. Commun.* **2018**, *9*, 2586.
(42) Madéo, J.; Man, M. K. L.; Sahoo, C.; Campbell, M.; Pareek, V.; Wong, E. L.; Al-Mahboob, A.; Chan, N. S.; Karmakar, A.; Mariserla, B. M. K.; Li, X.; Heinz, T. F.; Cao, T.; Dani, K. M. Directly Visualizing the Momentum-Forbidden Dark Excitons and Their Dynamics in Atomically Thin Semiconductors. *Science* **2020**, *370*, 1199−1204.
(43) Yuan, L.; Wang, T.; Zhu, T.; Zhou, M.; Huang, L. Exciton Dynamics, Transport, and Annihilation in Atomically Thin Two-Dimensional Semiconductors. *J. Phys. Chem. Lett.* **2017**, *8*, 3371−3379.
(44) Palummo, M.; Bernardi, M.; Grossman, J. C. Exciton Radiative Lifetimes in Two-Dimensional Transition Metal Dichalcogenides. *Nano Lett.* **2015**, *15*, 2794−2800.
(45) Delor, M.; Weaver, H. L.; Yu, Q.; Ginsberg, N. S. Imaging Material Functionality through Three-Dimensional Nanoscale Tracking of Energy Flow. *Nat. Mater.* **2020**, *19*, 56−62.
(46) Zhao, W.; Ribeiro, R. M.; Toh, M.; Carvalho, A.; Kloc, C.; Castro Neto, A. H.; Eda, G. Origin of Indirect Optical Transitions in Few-Layer $MoS_2$, $WS_2$, and $WSe_2$. *Nano Lett.* **2013**, *13*, 5627−5634.
(47) Haigh, S. J.; Gholinia, A.; Jalil, R.; Romani, S.; Britnell, L.; Elias, D. C.; Novoselov, K. S.; Ponomarenko, L. A.; Geim, A. K.; Gorbachev, R. Cross-Sectional Imaging of Individual Layers and Buried Interfaces of Graphene-Based Heterostructures and Superlattices. *Nat. Mater.* **2012**, *11*, 764−767.
(48) Khestanova, E.; Guinea, F.; Fumagalli, L.; Geim, A. K.; Grigorieva, I. V. Universal Shape and Pressure inside Bubbles Appearing in van Der Waals Heterostructures. *Nat. Commun.* **2016**, *7*, 12587.
(49) Tyurnina, A. V.; Bandurin, D. A.; Khestanova, E.; Kravets, V. G.; Koperski, M.; Guinea, F.; Grigorenko, A. N.; Geim, A. K.; Grigorieva, I. V. Strained Bubbles in van Der Waals Heterostructures as Local Emitters of Photoluminescence with Adjustable Wavelength. *ACS Photonics* **2019**, *6*, 516−524.
(50) Darlington, T. P.; Carmesin, C.; Florian, M.; Yanev, E.; Ajayi, O.; Ardelean, J.; Rhodes, D. A.; Ghiotto, A.; Krayev, A.; Watanabe, K.; Taniguchi, T.; Kysar, J. W.; Pasupathy, A. N.; Hone, J. C.; Jahnke, F.; Borys, N. J.; Schuck, P. J. Imaging Strain-Localized Excitons in Nanoscale Bubbles of Monolayer $WSe_2$ at Room Temperature. *Nat. Nanotechnol.* **2020**, *15*, 854−860.
(51) Carmesin, C.; Lorke, M.; Florian, M.; Erben, D.; Schulz, A.; Wehling, T. O.; Jahnke, F. Quantum-Dot-Like States in Molybdenum Disulfide Nanostructures Due to the Interplay of Local Surface Wrinkling, Strain, and Dielectric Confinement. *Nano Lett.* **2019**, *19*, 3182−3186.
(52) Edelberg, D.; Rhodes, D.; Kerelsky, A.; Kim, B.; Wang, J.; Zangiabadi, A.; Kim, C.; Abhinandan, A.; Ardelean, J.; Scully, M.; Scullion, D.; Embon, L.; Zu, R.; Santos, E. J. G.; Balicas, L.; Marianetti, C.; Barmak, K.; Zhu, X.; Hone, J.; Pasupathy, A. N. Approaching the Intrinsic Limit in Transition Metal Diselenides via Point Defect Control. *Nano Lett.* **2019**, *19*, 4371−4379.
(53) Tang, Y.; Li, L.; Li, T.; Xu, Y.; Liu, S.; Barmak, K.; Watanabe, K.; Taniguchi, T.; MacDonald, A. H.; Shan, J.; Mak, K. F. Simulation of Hubbard Model Physics in $WSe_2/WS_2$ Moiré Superlattices. *Nature* **2020**, *579*, 353−358.
(54) Lindfors, K.; Kalkbrenner, T.; Stoller, P.; Sandoghdar, V. Detection and Spectroscopy of Gold Nanoparticles Using Supercontinuum White Light Confocal Microscopy. *Phys. Rev. Lett.* **2004**, *93*, 037401.
(55) Taylor, R. W.; Sandoghdar, V. Interferometric Scattering Microscopy: Seeing Single Nanoparticles and Molecules via Rayleigh Scattering. *Nano Lett.* **2019**, *19*, 4827−4835.
(56) Ortega-Arroyo, J.; Kukura, P. Interferometric Scattering Microscopy (ISCAT): New Frontiers in Ultrafast and Ultrasensitive Optical Microscopy. *Phys. Chem. Chem. Phys.* **2012**, *14*, 15625−15636.
(57) Zhu, T.; Snaider, J. M.; Yuan, L.; Huang, L. Ultrafast Dynamic Microscopy of Carrier and Exciton Transport. *Annu. Rev. Phys. Chem.* **2019**, *70*, 219−244.
(58) Ginsberg, N. S.; Tisdale, W. A. Spatially Resolved Exciton and Charge Transport in Emerging Semiconductors. *Annu. Rev. Phys. Chem.* **2020**, *71*, 1−30.
(59) Guzelturk, B.; Utterback, J. K.; Coropceanu, I.; Kamysbayev, V.; Janke, E. M.; Zajac, M.; Yazdani, N.; Cotts, B. L.; Park, S.; Sood, A.; Lin, M.-F.; Reid, A. H.; Kozina, M. E.; Shen, X.; Weathersby, S. P.; Wood, V.; Salleo, A.; Wang, X.; Talapin, D. V.; Ginsberg, N. S.;


https://doi.org/10.1021/acs.nanolett.1c04997
*Nano Lett.* 2022, 22, 2843−2850

Lindenberg, A. M. Nonequilibrium Thermodynamics of Colloidal Gold Nanocrystals Monitored by Ultrafast Electron Diffraction and Optical Scattering Microscopy. *ACS Nano* **2020**, *14*, 4792−4804.
(60) Utterback, J. K.; Sood, A.; Coropceanu, I.; Guzelturk, B.; Talapin, D. V.; Lindenberg, A. M.; Ginsberg, N. S. Nanoscale Disorder Generates Subdiffusive Heat Transport in Self-Assembled Nanocrystal Films. *Nano Lett.* **2021**, *21*, 3540−3547.
(61) Goodman, A. J.; Willard, A. P.; Tisdale, W. A. Exciton Trapping Is Responsible for the Long Apparent Lifetime in Acid-Treated $MoS_2$. *Phys. Rev. B* **2017**, *96*, 1−6.
(62) Kulig, M.; Zipfel, J.; Nagler, P.; Blanter, S.; Schüller, C.; Korn, T.; Paradiso, N.; Glazov, M. M.; Chernikov, A. Exciton Diffusion and Halo Effects in Monolayer Semiconductors. *Phys. Rev. Lett.* **2018**, *120*, 207401.
(63) Cordovilla Leon, D. F.; Li, Z.; Jang, S. W.; Cheng, C.-H.; Deotare, P. B. Exciton Transport in Strained Monolayer $WSe_2$. *Appl. Phys. Lett.* **2018**, *113*, 252101.
(64) Ajayi, O. A.; Ardelean, J. V.; Shepard, G. D.; Wang, J.; Antony, A.; Taniguchi, T.; Watanabe, K.; Heinz, T. F.; Strauf, S.; Zhu, X.-Y.; Hone, J. C. Approaching the Intrinsic Photoluminescence Linewidth in Transition Metal Dichalcogenide Monolayers. *2D Mater.* **2017**, *4*, 031011.
(65) Rhodes, D.; Chae, S. H.; Ribeiro-Palau, R.; Hone, J. Disorder in van Der Waals Heterostructures of 2D Materials. *Nat. Mater.* **2019**, *18*, 541−549.
(66) Zipfel, J.; Kulig, M.; Perea-Causín, R.; Brem, S.; Ziegler, J. D.; Rosati, R.; Taniguchi, T.; Watanabe, K.; Glazov, M. M.; Malic, E.; Chernikov, A. Exciton Diffusion in Monolayer Semiconductors with Suppressed Disorder. *Phys. Rev. B* **2020**, *101*, 115430.
(67) Zhao, W.; Ghorannevis, Z.; Chu, L.; Toh, M.; Kloc, C.; Tan, P. H.; Eda, G. Evolution of Electronic Structure in Atomically Thin Sheets of $WS_2$ and $WSe_2$. *ACS Nano* **2013**, *7*, 791−797.
(68) Aslan, O. B.; Deng, M.; Heinz, T. F. Strain Tuning of Excitons in Monolayer $WSe_2$. *Phys. Rev. B* **2018**, *98*, 115308.
(69) Chang, C.-H.; Fan, X.; Lin, S.-H.; Kuo, J.-L. Orbital Analysis of Electronic Structure and Phonon Dispersion in $MoS_2$, $MoSe_2$, $WS_2$, and $WSe_2$ Monolayers under Strain. *Phys. Rev. B* **2013**, *88*, 195420.
(70) Carrascoso, F.; Li, H.; Frisenda, R.; Castellanos-Gomez, A. Strain Engineering in Single-, Bi- and Tri-Layer $MoS_2$, $MoSe_2$, $WS_2$ and $WSe_2$. *Nano Res.* **2021**, *14*, 1698−1703.
(71) Rosati, R.; Schmidt, R.; Brem, S.; Perea-Causín, R.; Niehues, I.; Kern, J.; Preuß, J. A.; Schneider, R.; Michaelis de Vasconcellos, S.; Bratschitsch, R.; Malic, E. Dark Exciton Anti-Funneling in Atomically Thin Semiconductors. *Nat. Commun.* **2021**, *12*, 7221.
(72) Feierabend, M.; Berghäuser, G.; Knorr, A.; Malic, E. Proposal for Dark Exciton Based Chemical Sensors. *Nat. Commun.* **2017**, *8*, 14776.
(73) Waldecker, L.; Raja, A.; Rösner, M.; Steinke, C.; Bostwick, A.; Koch, R. J.; Jozwiak, C.; Taniguchi, T.; Watanabe, K.; Rotenberg, E.; Wehling, T. O.; Heinz, T. F. Rigid Band Shifts in Two-Dimensional Semiconductors through External Dielectric Screening. *Phys. Rev. Lett.* **2019**, *123*, 206403.





https://doi.org/10.1021/acs.nanolett.1c04997
*Nano Lett.* 2022, 22, 2843−2850